Title

An optics-based variable-temperature assay system for characterizing thermodynamics of biomolecular reactions on solid support.

Journal

The Review of scientific instruments, 84(11)

ISSN

0034-6748

Authors

Fei, Yiyan
Landry, James P
Li, Yanhong
et al.

Publication Date

2013-11-01

DOI

10.1063/1.4826352

Peer reviewed

An optics-based variable-temperature assay system for characterizing thermodynamics of biomolecular reactions on solid support

Yiyan Fei,[1,a)] James P. Landry,[1] Yanhong Li,[2] Hai Yu,[2] Kam Lau,[2,b)] Shengshu Huang,[2] Harshal A. Chokhawala,[2,c)] Xi Chen,[2] and X. D. Zhu[1,d)]
[1]*Department of Physics, University of California, One Shields Avenue, Davis, California 95616, USA*
[2]*Department of Chemistry, University of California, One Shields Avenue, Davis, California 95616, USA*

(Received 9 August 2013; accepted 7 October 2013; published online 5 November 2013)

A biological state is equilibrium of multiple concurrent biomolecular reactions. The relative importance of these reactions depends on physiological temperature typically between 10 °C and 50 °C. Experimentally the temperature dependence of binding reaction constants reveals thermodynamics and thus details of these biomolecular processes. We developed a variable-temperature opto-fluidic system for real-time measurement of multiple (400–10 000) biomolecular binding reactions on solid supports from 10 °C to 60 °C within ±0.1 °C. We illustrate the performance of this system with investigation of binding reactions of plant lectins (carbohydrate-binding proteins) with 24 synthetic glycans (i.e., carbohydrates). We found that the lectin-glycan reactions in general can be enthalpy-driven, entropy-driven, or both, and water molecules play critical roles in the thermodynamics of these reactions. © *2013 AIP Publishing LLC*. [http://dx.doi.org/10.1063/1.4826352]

I. INTRODUCTION

Biomolecular binding reactions under physiological conditions and their equilibria (when concurrently present) are molecular processes that control cellular states, dynamics, and evolution. Understanding of these processes is central to molecular biology and is the basis of drug discovery. Two key components of physiological conditions are the temperature range (nominally from 10 °C to 50 °C or 283 K to 323 K) and the aqueous environment consisting of a host of molecules dissolved or suspended in water, in addition to the main reaction constituents of interest. Unlike most associative chemical reactions that are typically enthalpy-driven (i.e., dominated by the decrease in enthalpy ΔH) at the expense of decrease in entropy, associative reactions involving macromolecules such as proteins are often accompanied by conformational change, solvation/de-solvation, and entrapment of water or other solvent molecules. As a result, the spontaneous association can be entropy-driven when the overall change in entropy ΔS including those of the solvent is positive and dominates the net negative change in the Gibbs free energy ΔG ($=\Delta H - T\Delta S$).[1–15] It is clear that experimental studies of biomolecular binding reactions should be performed over the entire physiological temperature range instead of merely at room temperature around 300 K. By measuring equilibrium binding constants as a function of temperature, one can determine changes in Gibbs free energy G, enthalpy H, and entropy S (through Van't Hoff equation and other thermodynamic equations) and gain insights into other key molecular processes that accompany the main reaction. In practice these insights are useful in guiding drug design and optimization.

Commercial systems based on a range of techniques are available to characterize biomolecular binding reactions in solutions (e.g., Isothermal Titration Calorimetry and Differential Scanning Calorimetry[16–18]) or on solid supports (e.g., Surface Plasmon Resonance and interference sensors) as a function of temperature.[8] So far these platforms are limited to detecting a few to a few tens of reactions at a time over the entire physiological temperature range or to detection of a few hundreds of reactions but only at or above room temperature. In this report, we describe a variable-temperature ellipsometry-based assay system for simultaneously detecting 1000–10 000 reactions from 10 °C to 60 °C within ±0.1 °C.[19–22] Such a system enables us to measure temperature dependence and in turn the thermodynamics of biomolecular interactions with unprecedented throughput. Using this system, we studied interactions of plant carbohydrate-binding proteins (a.k.a. lectins) with 24 synthetic carbohydrates (a.k.a. glycans).[23]

II. VARIABLE-TEMPERATURE OPTO-FLUIDIC SYSTEM FOR REAL-TIME MEASUREMENT OF MULTIPLE BINDING REACTIONS ON A SOLID SUPPORT

A. Variable-temperature opto-fluidic system

The system consists of a temperature-controlled sample cartridge and a scanning ellipsometry microscope. The novel component here is the sample cartridge as shown in Figure 1. It consists of a titanium plate fabricated to house either one large fluidic chamber[24] or six smaller chambers. The glass slide printed with microarray(s) and the titanium plate are held together by an aluminum cap and through silicone O-ring(s) to form one large chamber or six smaller chambers with respective fluidic inlets and outlets. The space between the titanium plate and the glass slide is 0.4 mm.

[a)]Also at School of Information Science and Engineering, Fudan University, 220 Handan Road, Shanghai 200433, China.
[b)]Present address: Institute for Glycomics, Griffith University, Parklands Drive, Southport Qld 4215, Australia.
[c)]Present address: The Energy Biosciences Institute, University of California, 2151 Berkeley Way, Berkeley, California 94704, USA.
[d)]Electronic mail: xdzhu@physics.ucdavis.edu. Tel.: +1 530-752-4689. Fax: +1 530-752-4717.

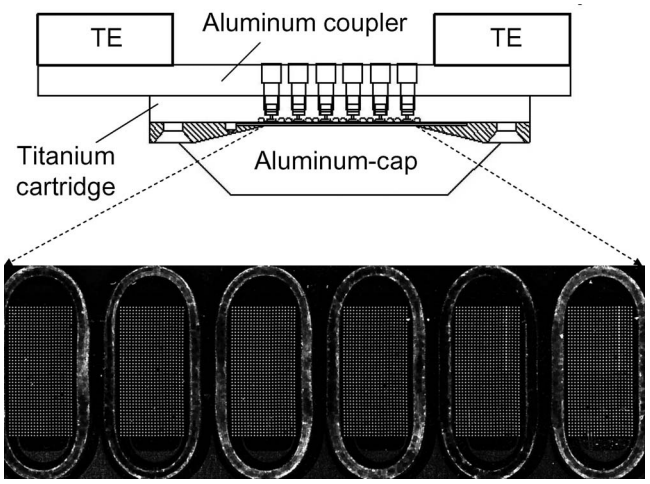

FIG. 1. Cross-sectional side-view of a temperature-controlled multi-chamber assembly (integrated with an oblique-incidence reflectivity difference microscope that is not shown here. See Figure 1 of Ref. 20). **Aluminum coupler** thermally joints two thermoelectric units (TE, from a commercial vendor) to **Titanium cartridge** that houses 6 planar chambers. **Aluminum-cap** holds a 1 in. × 3 in. printed glass slide on **Titanium cartridge** to complete the fluid chambers. A thermocouple (not shown) is mounted 0.4 mm behind one of the fluidic chambers to monitor the temperature of the titanium surface. The assembly enables binding assays between 10 °C and 60 °C within ±0.1 °C. The insert is an image of six bovine serum albumin (BSA) microarrays printed on an epoxy-functionalized glass slide in aqueous solution. Each microarray has 800 spots with a diameter of 100 μm. The image is acquired with the integrated microscope.

The aluminum cap has a 20-mm × 44-mm rectangular opening so that the optical beam from the scanning microscope has the access to the microarray(s) from the opposite side of the glass slide at an incidence angle of 65°. The cap also has a pair of 20-mm wide × 60-mm long shields above and below the exposed glass slide surface to minimize convective air movement during experiment, which is an important element of the design.

B. Temperature control

To vary the temperature of the microarray on the glass surface in the physiological range, we take the thermoelectric heating/cooling component from a commercial thermal stage (TSA02i, INSTEC Inc, Boulder, CO) and outfit it to an aluminum adapter that is held in good thermal contact with the titanium plate. For temperature control feedback, a thermocouple is placed through a 1.5-mm-diameter hole and held in good thermal contact with the back of the titanium plate at 0.5 mm from the fluid chamber surface. The reading of the thermocouple T_{set} is used as the temperature of the microarray surface and the feedback for the TSA02i control electronics. The titanium plate temperature T_{set} can be varied from 10 °C to 60 °C within ±0.1 °C. Once T_{set} is set, the fluidic assembly reaches the equilibrium with the ambient in 5–10 min and the aqueous buffer and the glass slide also reach respective steady-state temperatures that are very close to T_{set} (see below for further analysis). In a typical binding reaction experiment, an aqueous sample at ambient temperature is injected into the reaction chamber through the inlet to replace the buffer in 1–2 s. With the high thermal conductivity of titanium (∼5 cal/s m °C) and the shallow reaction chamber depth of 0.4 mm, it is easily shown that the injected solution reaches a steady-state temperature T_{sample} within 0.1° in less than 2 s. And we show next that T_{sample} is essentially the same as T_{set}.

C. Microarray temperature T_{sample} vs. the titanium plate temperature T_{set}

The glass surface printed with microarray(s) is 0.4 mm (the depth of the reaction chamber d_{ch}) from the titanium surface where the temperature T_{set} is being set and monitored. T_{sample} is determined by the titanium plate temperature T_{set}, the ambient temperature $T_{ambient}$, and the geometry of the assembly. Under the steady-state condition, the temperature variation across the chamber depth is a linear function of the distance away from the titanium surface. Let d_{glass} be the thickness of the glass slide and $d_{ambient}$ the normal distance between the front surface of the glass slide and the ambient location where the temperature linearly reaches $T_{ambient}$. Let thermal conductivities of a typical aqueous solution, a glass slide, and the ambient air be k_{aqua}, k_{glass}, and k_{air}. It is easy to show that the temperature at the microarray surface is given by

$$T_{sample} = T_{set} + \frac{(T_{ambient} - T_{set})\, d_{ch}}{(k_{aqua}/k_{glass})\, d_{glass} + (k_{aqua}/k_{air})\, d_{ambient} + d_{ch}}. \quad (1)$$

In our present system, $d_{ch} = 0.4$ mm, $d_{glass} = 2$ mm, $k_{aqua}/k_{glass} = 0.5$, $k_{aqua}/k_{air} = 20$, $|T_{ambient} - T_{set}| \sim 20$ °C. In the absence of convection in front of the glass slide due to the aluminum shields, we expect $d_{ambient} > 10$ mm. As a result we expect in steady-state, $T_{sample} = T_{set} \pm 0.1$ °C. It means that the temperature at the microarray surface T_{sample} is practically the same as that of the titanium plate T_{set} within 2 s after the aqueous solution is injected into the chamber.

D. Scanning ellipsometry microscope

The main features of the microscope have been described previously.[19,20,22] Briefly, the microscope measures the oblique-incidence reflectivity difference (OI-RD signal) defined as the difference in fractional reflectivity change between the *p*-polarized and *s*-polarized components of a monochromatic light (a He-Ne laser in the present case) when reflecting off a microarray-covered glass surface, $(r_p - r_{p0})/r_{p0} - (r_s - r_{s0})/r_{s0} \equiv \Delta_p - \Delta_s$. r_{p0} and r_{s0} are the complex reflectivities of the bare glass surface; r_p and r_s are the reflectivities of the glass surface when it is covered with an immobilized molecular layer. It has been shown that[22]

$$\Delta_p - \Delta_s \cong -i \left[\frac{4\pi \varepsilon_s (\tan\phi_{inc})^2 \cos\phi_{inc}}{\varepsilon_0^{1/2} (\varepsilon_s - \varepsilon_0)\left(\varepsilon_s/\varepsilon_0 - (\tan\phi_{inc})^2\right)} \right] \times \frac{(\varepsilon_d - \varepsilon_s)(\varepsilon_d - \varepsilon_0)\,\Theta}{\varepsilon_d} \left(\frac{d}{\lambda}\right), \quad (2)$$

ϕ_{inc} is the incidence angle of the monochromatic light beam. ε_0, ε_d, and ε_s are respective optical dielectric constants of the

glass slide, the immobilized molecular layer, and the aqueous ambient. λ (= 632.8 nm) is the wavelength of the monochromatic illuminating light. d is the thickness of the molecular layer. Θ is the coverage of the molecular layer, defined as the quotient of the surface area actually covered by the molecules in the layer divided by the footprint of the layer. $\Delta_p - \Delta_s$ is proportional to the surface mass density $\Gamma = \Theta d \rho_{protein}$ of the molecular layer ($\rho_{protein} = 1.35$ g/cm^3 is the volume mass density of protein in an aqueous ambient).[19,22] Since the glass substrate, the aqueous ambient, and the immobilized molecular layer are transparent at the wavelength of the monochromatic light source ($\lambda = 632.8$ nm), ε_0, ε_s, and ε_d are real numbers. As a result only $\mathrm{Im}\{\Delta_p - \Delta_s\}$ is non-zero,

$$\mathrm{Im}\left\{\Delta_p - \Delta_s\right\} = -\left[\frac{4\pi\varepsilon_s(\tan\phi_{inc})^2\cos\phi_{inc}}{\varepsilon_0^{1/2}(\varepsilon_s-\varepsilon_0)\left(\varepsilon_s/\varepsilon_0-(\tan\phi_{inc})^2\right)}\right] \times\frac{(\varepsilon_d-\varepsilon_s)(\varepsilon_d-\varepsilon_0)\Theta}{\varepsilon_d}\left(\frac{d}{\lambda}\right). \quad (3)$$

We only measure $\mathrm{Im}\{\Delta_p - \Delta_s\}$ when detecting binding reactions of lectins with carbohydrate (glycan) microarrays.

III. APPLICATION TO TEMPERATURE-DEPENDENCE STUDIES OF PROTEIN-CARBOHYDRATE (LECTIN-GLYCAN) BINDING

Protein-carbohydrate binding reactions are prototypical for investigation of temperature dependence of biomolecular interactions. For example, through surface membrane proteins, viral particles interact distinctly with specific and non-specific hosts that have different characteristic physiological temperatures (e.g., human vs. avian). Generally, spontaneous association of a protein molecule with ligands such as carbohydrates, peptides, or low-molecular-weight compounds may not always be driven by a predominant decrease in enthalpy at the expense of entropy. As the protein molecule is prone to conformational change and to the change in the state of solvation due to hydrophobic interaction for example, the association of the protein with a ligand can proceed with an increase in entropy so that the protein-ligand complex may become more stable at higher temperature instead of the opposite. In these cases, the entropy gain is indicative of other important structural and in turn entropic changes that may be equally significant as the association reaction itself. To access these details in protein-ligand interactions, one needs to determine equilibrium binding constants as a function of temperature and extract changes in Gibbs free energy, enthalpy, and entropy through Van't Hoff equation.

Figure 2 shows the structures of 24 synthetic oligosaccharides or carbohydrates (OS-1 to OS-24) used in this study: four β1-4-linked galactosides, three β1-3-linked galactosides, one shorter β-galactoside, one α-linked *N*-acetylgalactosaminide, eight α2-3-linked sialosides, and seven α2-6-linked sialosides.[23] Table I lists these carbohydrates. All glycans are linked to biotin via a flexible hexa(ethylene glycol) HEG linker to allow optimal presentation of glycans to subsequent lectins in binding assays by immobilizing biotinylated glycans on streptavidin-functionalized glass surface. Lectins used were *Ricinu communis* Agglutinin (RCA, 120 kDa), *Maackia amurensis* Agglutinin (MAA, 130 kDa), and *Sambucus nigra* Bark Agglutinin (SNA, 150 kDa), all were purchased from Vector Laboratories (Burlingame, CA). The lectins were diluted with 1 × phosphate buffered saline (PBS) to concentrations in the range of μM for real-time binding affinity measurement. The binding profiles of these three lectins to the same 24 carbohydrates at room temperature have been reported earlier.[23]

We measured binding curves of MAA, RCA, and SNA to all 24 carbohydrates at 15 °C, 25 °C, 35 °C, and 45 °C at three lectin concentrations (MAA: 0.75 μM, 1.5 μM, and 3.0 μM; SNA: 0.39 μM, 0.78 μM, 1.57 μM; RCA: 0.84 μM, 1.67 μM, 3.33 μM). In terms of absolute temperature, the largest temperature change was 10%. Figure 3 displays the binding curves of MAA but only to 7 carbohydrates (OS-11 through OS-17) as the ones to the remaining 17 carbohydrates show no sign of binding at the concentrations used in the experiments. Figure 4 displays the binding curves to 7 carbohydrates (OS-18 through OS-24) as the ones to the first 17 carbohydrates show no sign of SNA binding. Figure 5 displays the binding curves of RCA to all 24 carbohydrates. The optical signals are proportional to the surface mass density change as a result of the lectin binding.

Before detailed analysis, two features are immediately obvious. Most binding curves are not described by a simple 1-to-1 (one-site) Langmuir reaction model, indicating that the bound lectin-carbohydrate pair on the solid support forms more than one type of complexes, each with a distinct binding constant or association and dissociation rate constants.[25] The stability of many lectin-carbohydrate complexes decreases with the increase of the temperature when the latter changes from 15 °C to 45 °C (a hallmark of enthalpy-driven reaction), while there are clearly complexes whose stabilities depend weakly on temperature. The stabilities of some complexes even increase with the rise of the temperature (a clear sign of entropy-favored reaction).

To gain further insights into the lectin-glycan binding (complex formation), we fit the binding curves obtained at a constant temperature and three difference lectin concentrations globally to a two-site Langmuir reaction model.[25] In this model, we assume that there are two presentations for each immobilized carbohydrate ligand, and the binding of a lectin with these two presentations leads to a primary complex and a secondary complex that are characterized by distinct association rate constants and dissociation rate constants: $k_{on}^{(1)}$, $k_{on}^{(2)}$, $k_{off}^{(1)}$, and $k_{off}^{(2)}$. We use these rate constants as global fitting parameters and use initial surface densities $N_0^{(1)}$ and $N_0^{(2)}$ of the two carbohydrate presentations (sites) as the local parameters that can vary from binding curve to binding curve. We then compute the equilibrium association constants $K_a^{(1)} = k_{on}^{(1)}/k_{off}^{(1)}$ and $K_a^{(2)} = k_{on}^{(2)}/k_{off}^{(2)}$. To find thermodynamic parameters associated with these binding reactions, we use the following equations: (1) reaction isotherm $\Delta G = -(RT)\,Ln(K_a)$; (2) Van't Hoff equation $\Delta H = (RT^2)\,dLn(K_a)/dT$; and (3) definition of Gibbs free

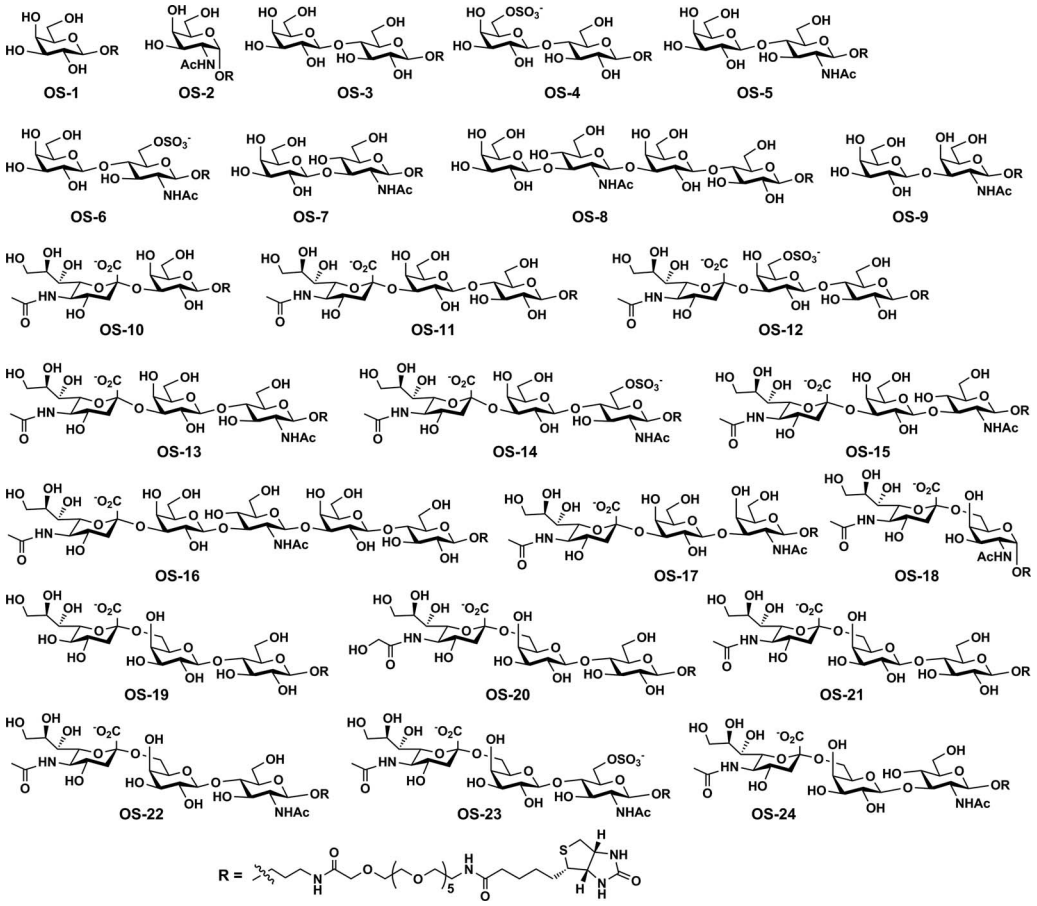

FIG. 2. Structures of 24 synthetic biotinylated oligosaccharides (galactosides, *N*-acetylgalactosaminide, and sialosides). Except for OS-2 and OS-18 which are α-linked to a biotin linker, all other glycans are β-linked to biotin via a flexible hexa(ethylene glycol) (HEG) linker.

energy change $\Delta G = \Delta H - T\Delta S$ or $\Delta S = (\Delta H - \Delta G)/T$. We have assumed that over the narrow temperature range between 15 °C and 45 °C or from 288 K to 318 K, the dependence in enthalpy change ΔH and entropy change ΔS on temperature can be neglected. In Table II, we list equilibrium association constants and thermal dynamic parameters of MAA and SNA binding reactions with respective synthetic glycans (see Figures 3 and 4). Table III displays equilibrium association constants and thermal dynamic parameters of RCA binding reactions with the synthetic glycans (see Figure 5).

A. MAA-glycan binding reactions

MAA is known to bind to Neu5Acα2-3Galβ-terminated glycans (α2-3-linked sialosides). Yet thermodynamic driving forces behind MAA-glycan formation are not fully investigated. Earlier binding curve measurements at room temperature (~298 K) by others based on surface plasmon resonance (SPR) sensors yielded association constants in the order of 10^6/M, similar to what we found for the secondary MAA-Neu5Acα2-3Galβ complexes.[26] We note that the SPR-based measurements should have been analyzed with a two-site Langmuir reaction model as the data clearly indicated the presence of another more stable MAA-glycan complex. Our temperature dependence study of equilibrium association constants reveals the thermodynamics of MAA-glycan reactions. From Table II, one can see that the formation of secondary MAA-Neu5Acα2-3Galβ complexes is assisted by an entropy gain ($\Delta S > 0$). For MAA-Neu5Acα2-3Galβ1-4Glc/GlcNAcβ (OS-11 and OS-13) in particular, the entropy gain in fact drives the complex formation as the enthalpy change is positive and thus alone would render the complex formation unfavorable. For formation of primary (more stable) MAA-Neu5Acα2-3Galβ complexes, two of them are also assisted with entropy gain ($\Delta S > 0$).

B. SNA-glycan binding reactions

SNA is known to bind to Neu5Acα2-6Galβ-terminated glycans (α2-6-linked sialosides). The equilibrium association constants of secondary SNA-Neu5Acα2-6Galβ complexes found in the present study are comparable to those reported by others from SPR-based binding curve measurements at room temperature.[26] The temperature dependence of the

TABLE I. 24 Biotinylated oligosaccharides and the assigned identification numbers used in the present work.

Glycan I.D.	Glycan structures				
OS-1		Gal	β-Biotin		
OS-2		GalNAc	α-Biotin		
OS-3		Gal	β1-4Glc	β-Biotin	
OS-4		Gal6S	β1-4Glc	β-Biotin	
OS-5		Gal	β1-4GlcNAc	β-Biotin	
OS-6		Gal	β1-4GlcNAc6S	β-Biotin	
OS-7		Gal	β1-3GlcNAc	β-Biotin	
OS-8		Gal	β1-3GlcNAc	β1-3Galβ1-4Glc	β-Biotin
OS-9		Gal	β1-3GalNAc	β-Biotin	
OS-10	Neu5Acα2-3	Gal	β-Biotin		
OS-11	Neu5Acα2-3	Gal	β1-4Glc	β-Biotin	
OS-12	Neu5Acα2-3	Gal6S	β1-4Glc	β-Biotin	
OS-13	Neu5Acα2-3	Gal	β1-4GlcNAc	β-Biotin	
OS-14	Neu5Acα2-3	Gal	β1-4GlcNAc6S	β-Biotin	
OS-15	Neu5Acα2-3	Gal	β1-3GlcNAc	β-Biotin	
OS-16	Neu5Acα2-3	Gal	β1-3GlcNAc	β1-3Galβ1-4Glc	β-Biotin
OS-17	Neu5Acα2-3	Gal	β1-3GalNAc	β-Biotin	
OS-18	Neu5Acα2-6	GalNAc	α-Biotin		
OS-19	Kdnα2-6	Gal	β1-4Glc	β-Biotin	
OS-20	Neu5Gcα2-6	Gal	β1-4Glc	β-Biotin	
OS-21	Neu5Acα2-6	Gal	β1-4Glc	β-Biotin	
OS-22	Neu5Acα2-6	Gal	β1-4GlcNAc	β-Biotin	
OS-23	Neu5Acα2-6	Gal	β1-4GlcNAc6S	β-Biotin	
OS-24	Neu5Acα2-6	Gal	β1-3GlcNAc	β-Biotin	

equilibrium association constants again allows us to examine the thermodynamics in forming these lectin-glycan complexes. From Table II, we find that the binding of SNA to Neu5Acα2-6Galβ-terminated glycans is primarily driven by an enthalpy decrease as the latter contributes to the bulk of the negative change in Gibbs free energy (required for spontaneous complex formation). Interestingly, the formation of the secondary SNA-Kdnα2-6Galβ (OS-19) complex as well as the primary SNA-Neu5Acα2-6Galβ1-4Glcβ (OS-21) and SNA-Neu5Acα2-6Galβ1-4GlcNAc6Sβ (OS-23) complexes is also assisted by an entropy gain ($\Delta S > 0$), while the formation of other SNA-Neu5Acα2-6Galβ complexes results in an entropy loss ($\Delta S < 0$).

C. RCA-glycan binding reaction

RCA binds to Galβ1-3/4- and Neu5Acα2-6Galβ1-3/4-terminated glycans. From the temperature dependence of the equilibrium association constants in Table III, we can conclude that the formation of primary RCA-Galβ1-4Glc/GlcNAc (OS-3 and OS-5) complexes are driven by entropy gains as the enthalpy loss only contributes to a

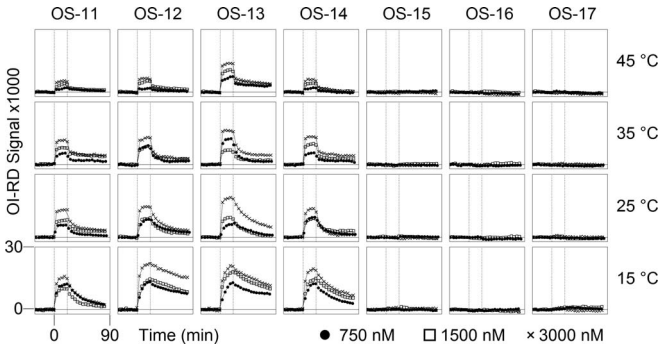

FIG. 3. Temperature dependence of binding curves (association-dissociation curves) of *Maackia amurensis* Agglutinin (MAA) to glycans immobilized on streptavidin-functionalized surface at three MAA concentrations. Only those for OS-11 through OS-17 are shown as MAA does not bind to other glycans. The curves are fitted to a two-site Langmuir reaction model.

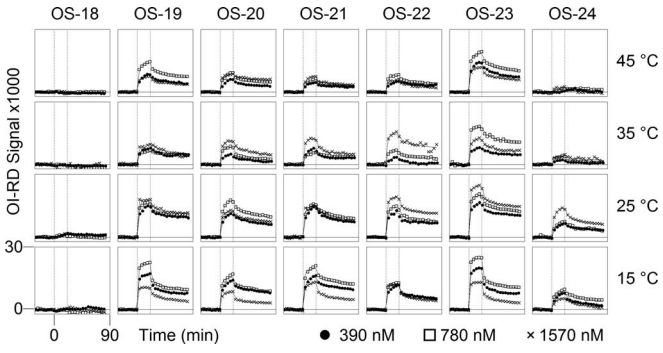

FIG. 4. Binding curves (association-dissociation curves) of *Sambucus nigra* Bark Agglutinin (SNA) to glycans immobilized on streptavidin-functionalized surface at three SNA concentrations. Only those for OS-18 through OS-24 are shown as SNA does not bind to other glycans. The curves are fitted to a two-site Langmuir reaction kinetic model.

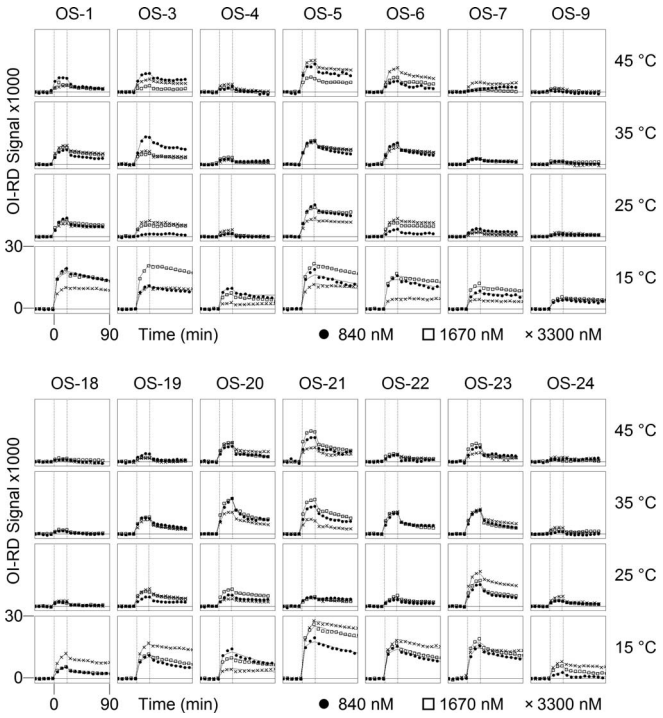

FIG. 5. Binding curves (association-dissociation curves) of RCA (*Ricinu communis* Agglutinin) to glycans immobilized on streptavidin-functionalized surface at three RCA concentrations. The curves for those glycans that do not bind RCA are not shown. The curves are fitted to a two-site Langmuir reaction kinetic model.

minor portion of the Gibbs free energy loss, while the formation of primary RCA-Galβ1-3GlcNAac/GalNAc (OS-7 and OS-9) complexes is completely driven by the enthalpy loss since the entropy decreases as a result of the complex formation. For RCA-Neu5Acα2-6Galβ1-3/4 complexes, the formation is dominated by the enthalpy loss. Interestingly, when Neu5Ac group is replaced by Kdn group or when Neu5Acα2-6Galβ1-4GlcNAc (OS-22) is modified to Neu5Acα2-6Galβ1-4GlcNAc6S (OS-23), RCA binding to the modified glycans is now accompanied by entropy gains ($\Delta S > 0$).

IV. DISCUSSION

Protein-ligand binding reactions, such as those between lectins and glycans, in aqueous solutions are accompanied by solvation and de-solvation of structured/perturbed water molecules and/or other solvents in the binding pocket or on the binding surface. As a result, the Gibbs free energy change that drives the complex formation can have significant contributions from the bound water or other solvent molecules. In particular, when the numbers of solvent molecules on the respective binding surfaces of a lectin and a glycan are large, the entropic gain in releasing some or all of these molecules into the bulk can dominate the thermodynamic force that stabilizes the complex formation (entropy-driven reaction). The theoretical consideration and experimental observation of these concepts have been explored and investigated by Lemieux and others for a number of lectin-glycan reactions and other protein-ligand binding reactions.[1–15] In general, the net entropy gain can be regarded a measure of the amount of the bound water molecules released in the complex formation as the displacement of one bound water molecule into the bulk decreases the Gibbs free energy by 1–2 kcal/mol at room temperature.

From this consideration, it is clear that the binding of MAA to Neu5Acα2-3Galβ1-4GlcNAcβ involves displacements of a large number of bound water molecules (6–10) from binding surfaces of MAA and glycans. When *N*-acetylglucosamine is replaced with glucose, only the secondary MAA-Neu5Acα2-3Galβ1-4Glcβ complex formation involves a large number of bound water molecules, while the primary complex formation involves far fewer bound water molecules ($\sim$1). The structural information on MAA-Neu5Acα2-3Galβ1-4Glc complex is available from the X-ray crystallography.[27] As shown in Figure 6, the binding pocket of MAA for Neu5Acα2-3Galβ1-4Glc is shaped like a cleft, a convenient pocket for structured water molecules. It is noteworthy that the surface region of MAA that binds to Galβ1-4Glc is mostly hydrophobic and as a result a small structural modification from Neu5Acα2-3Galβ1-4Glc to Neu5Acα2-3Galβ1-4GlcNAcβ can understandably lead to a large difference in bound water molecule displacement.

Though the structural information on SNA is also available[28], the binding pocket for Neu5Acα2-6Galβ is not known and thus we cannot comment on the correlation of the binding surface of SNA with our observation that the reactions of SNA with Neu5Acα2-6Galβ are mostly enthalpy driven and in some cases involve entropy gain. Unlike MAA, the surface of SNA seems readily covered with a layer of waters, indicating that the surface is much more hydrophilic. The formation of SNA with *N*-acetylgalactosamine complex retains most of the water molecules on SNA surface. According to Lemieux, the structured water layer on a hydrophilic or polar surface is perturbed and as a result the formation of SNA-glycan complex in most cases is expected to be enthalpy-driven instead of entropy-driven. This is what we observed.

The structure of RCA (Figure 7) is known as well and there is a large cleft-like pocket on the protein surface,[29] yet the structural details of RCA complexation with Galβ1-4Glc/GlcNAc, Galβ1-3Glc/GlcNAc, Neu5Acα2-6Galβ1-4, and Neu5Acα2-6Galβ1-3 are not available. It is feasible that Galβ1-4Glc/GlcNAc binds to the cleft-like pocket and displaces a large amount of structured water molecules in the formation of MAA-α2-3-linked sialoside complex such that the association with RCA is entropy-driven, while Galβ1-3Glc/GlcNAc binds to the same pocket but fits differently enough that fewer water molecules from the hydrophobic part of the cleft are displaced, leading to enthalpy-driven complex formation with RCA.

For the purpose of the present report, the interpretation of why some of the lectin-glycan reactions are entropy-driven, while others are dominated by enthalpy loss is tentative and subject to further study and confirmation. More importantly, our present variable-temperature assay system enables us to take a substantial step forward in revealing details of

TABLE II. Equilibrium association constants of MAA and SNA with sialyllactoses and sialyllactosamines between 15 °C and 45 °C, and the changes in thermodynamic functions during the complex formation deduced from the temperature dependence of the association constants. The bold face highlights those complexes whose formation is accompanied by a significant entropy gain.

MAA									
		Site 1				Site 2			
Glycan	T (K)	$K_a^{(1)}$ (1/M)	$\Delta G^{(1)}$ (kcal)	$\Delta H^{(1)}$ (kcal)	$\Delta S^{(1)}$ (kcal/K)	$K_a^{(2)}$ (1/M)	$\Delta G^{(2)}$ (kcal)	$\Delta H^{(2)}$ (kcal)	$\Delta S^{(2)}$ (kcal/K)
Neu5Acα3Galβ4Glc (OS-11)	288	2.3×10^7	−9.76	−10.2	-2.0×10^{-3}	1.2×10^6	−8.73	**4.3**	$\mathbf{4.2 \times 10^{-2}}$
	298	3.8×10^7	−10.40	−10.2	1.3×10^{-3}	2.0×10^6	−8.96	**4.3**	$\mathbf{4.3 \times 10^{-2}}$
	308	3.0×10^7	−10.61	−10.2	0.6×10^{-3}	3.4×10^6	−8.94	**4.3**	$\mathbf{4.5 \times 10^{-2}}$
	318	3.4×10^6	−9.56	−10.2	-1.6×10^{-3}	3.8×10^6	−8.90	**4.3**	$\mathbf{4.5 \times 10^{-2}}$
Neu5Acα3Gal6Sβ4Glc (OS-12)	288	4.0×10^8	−11.41	−11.4	6.5×10^{-5}	2.0×10^6	−8.36	−3.4	$\mathbf{1.7 \times 10^{-2}}$
	298	1.5×10^7	−9.85	−11.4	-5.2×10^{-3}	6.6×10^6	−9.36	−3.4	$\mathbf{2.1 \times 10^{-2}}$
	308	6.9×10^7	−11.12	−11.4	-0.88×10^{-3}	4.1×10^6	−9.38	−3.4	$\mathbf{1.9 \times 10^{-2}}$
	318	3.2×10^7	−10.99	−11.4	-1.3×10^{-3}	1.2×10^6	−8.90	−3.4	$\mathbf{1.7 \times 10^{-2}}$
Neu5Acα3Galβ4GlcNAc (OS-13)	288	2.1×10^8	−11.04	−7.7	$\mathbf{1.2 \times 10^{-2}}$	1.4×10^6	−8.14	3.3	$\mathbf{4.0 \times 10^{-2}}$
	298	1.4×10^7	−9.82	−7.7	$\mathbf{0.72 \times 10^{-2}}$	6.6×10^6	−9.36	3.3	$\mathbf{4.2 \times 10^{-2}}$
	308	7.0×10^7	−11.13	−7.7	$\mathbf{1.1 \times 10^{-2}}$	3.5×10^6	−9.28	3.3	$\mathbf{4.1 \times 10^{-2}}$
	318	3.2×10^7	−11.00	−7.7	$\mathbf{1.0 \times 10^{-2}}$	3.0×10^6	−9.48	3.3	$\mathbf{4.0 \times 10^{-2}}$
Neu5Acα3Galβ4GlcNAc6S (OS-14)	288	8.0×10^6	−9.16	−2.6	$\mathbf{2.3 \times 10^{-2}}$	2.5×10^6	−8.49	−3.5	$\mathbf{1.7 \times 10^{-2}}$
	298	6.0×10^6	−9.30	−2.6	$\mathbf{2.3 \times 10^{-2}}$	1.5×10^6	−8.48	−3.5	$\mathbf{1.7 \times 10^{-2}}$
	308	3.0×10^7	−10.61	−2.6	$\mathbf{2.6 \times 10^{-2}}$	1.3×10^6	−8.67	−3.5	$\mathbf{1.7 \times 10^{-2}}$
	318	2.8×10^6	−9.44	−2.6	$\mathbf{2.2 \times 10^{-2}}$	1.4×10^6	−9.00	−3.5	$\mathbf{1.7 \times 10^{-2}}$
SNA									
		Site 1				Site 2			
Glycan	T (K)	$K_a^{(1)}$ (1/M)	$\Delta G^{(1)}$ (kcal)	$\Delta H^{(1)}$ (kcal)	$\Delta S^{(1)}$ (kcal/K)	$K_a^{(2)}$ (1/M)	$\Delta G^{(2)}$ (kcal)	$\Delta H^{(2)}$ (kcal)	$\Delta S^{(2)}$ (kcal/K)
Kdnα6Galβ4Glc (OS-19)	288	8.0×10^8	−11.81	−19.2	-2.6×10^{-2}	2.9×10^5	−7.25	−7.2	1.9×10^{-4}
	298	5.3×10^8	−11.97	−19.2	-2.4×10^{-2}	4.9×10^7	−10.56	−7.2	1.1×10^{-2}
	303	5.7×10^7	−11.00	−19.2	-2.7×10^{-2}	4.2×10^7	−10.81	−7.2	1.2×10^{-2}
	318	5.1×10^7	−11.29	−19.2	-2.5×10^{-2}	2.3×10^7	−10.78	−7.2	1.1×10^{-2}
Neu5Gcα6Galβ4Glc (OS-20)	288	7.7×10^7	−10.46	−20	-3.3×10^{-2}	4.9×10^6	−8.87	−12	-1.1×10^{-2}
	298	3.0×10^7	−10.27	−20	-3.3×10^{-2}	6.7×10^6	−9.37	−12	-0.88×10^{-2}
	308	7.9×10^6	−9.79	−20	-3.3×10^{-2}	3.4×10^6	−9.26	−12	-0.89×10^{-2}
	318	2.7×10^7	−10.88	−20	-2.9×10^{-2}	1.9×10^6	−9.19	−12	-0.88×10^{-2}
Neu5Acα6Galβ4Glc (OS-21)	288	7.7×10^7	−12.06	−8.4	$\mathbf{7.2 \times 10^{-3}}$	2.6×10^6	−8.51	−12	-1.2×10^{-2}
	298	5.9×10^7	−10.66	−8.4	$\mathbf{7.6 \times 10^{-3}}$	2.8×10^7	−10.22	−12	-0.60×10^{-2}
	308	4.5×10^7	−10.86	−8.4	$\mathbf{8.0 \times 10^{-3}}$	3.1×10^6	−9.20	−12	-0.91×10^{-2}
	318	1.8×10^7	−10.62	−8.4	$\mathbf{7.0 \times 10^{-3}}$	5.6×10^5	−8.42	−12	-1.1×10^{-2}
Neu5Acα6Galβ4GlcNAc (OS-22)	288	4.1×10^8	−11.43	−16.3	-1.7×10^{-3}	8.6×10^5	−7.87	−13	-1.8×10^{-2}
	298	1.0×10^8	−10.97	−16.3	-1.8×10^{-3}	4.2×10^5	−7.71	−13	-1.8×10^{-2}
	308	6.6×10^7	−11.09	−16.3	-1.7×10^{-3}	5.0×10^6	−9.50	−13	-1.1×10^{-2}
	318	1.7×10^8	−12.06	−16.3	-1.3×10^{-3}	1.0×10^5	−7.34	−13	-1.8×10^{-2}
Neu5Acα6Galβ4GlcNAc6S (OS-23)	288	8.3×10^8	−11.83	−8.5	$\mathbf{1.3 \times 10^{-2}}$	3.7×10^5	−7.38	−9.3	-6.7×10^{-3}
	298	1.2×10^9	−12.42	−8.5	$\mathbf{1.3 \times 10^{-2}}$	1.2×10^5	−6.98	−9.3	-7.8×10^{-3}
	308	8.3×10^8	−12.65	−8.5	$\mathbf{1.3 \times 10^{-2}}$	1.0×10^5	−7.11	−9.3	-7.1×10^{-3}
	318	4.5×10^8	−12.68	−8.5	$\mathbf{1.2 \times 10^{-2}}$	0.73×10^5	−7.12	−9.3	-6.7×10^{-3}
Neu5Acα6Galβ3GlcNAc (OS-24)	288	3.1×10^8	−11.26	−24	-4.4×10^{-2}	6.4×10^4	−6.37	−16	-3.3×10^{-2}
	298	1.7×10^7	−9.93	−24	-4.7×10^{-2}	3.6×10^6	−8.99	−16	-2.4×10^{-2}
	308	2.1×10^7	−10.38	−24	-4.4×10^{-2}	2.3×10^5	−7.62	−16	-2.7×10^{-2}
	318	0.98×10^7	−8.77	−24	-4.8×10^{-2}	7.3×10^3	−5.66	−16	-3.3×10^{-2}

lectin-glycan or protein-ligand binding events under aqueous conditions and to investigate roles of water and other solvent molecules through measurements and analysis of the temperature dependence of equilibrium binding constants. The much-improved throughput of this platform promises to more rapidly advance the characterization of protein-ligand binding properties under various physiological conditions.

TABLE III. Equilibrium association constants of RCA with galactosides, galactosamine, and sialosides between 15 °C and 45 °C and the changes in thermodynamic functions during the complex formation computed from the temperature dependence of the association constants. The bold face highlights those complexes whose formation is accompanied by a significant entropy gain.

		RCA							
		Site 1				Site 2			
Glycan	T (K)	$K_a^{(1)}$ (1/M)	$\Delta G^{(1)}$ (kcal)	$\Delta H^{(1)}$ (kcal)	$\Delta S^{(1)}$ (kcal/K)	$K_a^{(2)}$ (1/M)	$\Delta G^{(2)}$ (kcal)	$\Delta H^{(2)}$ (kcal)	$\Delta S^{(2)}$ (kcal/K)
Gal (OS-1)	288	1.35×10^8	−10.78	−11.6	-2.8×10^{-3}	3.97×10^6	−8.75	−4.3	**1.5×10^{-2}**
	298	5.88×10^7	−10.66	−11.6	-3.2×10^{-3}	2.65×10^6	−8.81	−4.3	**1.5×10^{-2}**
	308	1.85×10^7	−10.31	−11.6	-4.2×10^{-3}	2.44×10^6	−9.06	−4.3	**1.5×10^{-2}**
	318	2.44×10^7	−10.82	−11.6	-1.8×10^{-3}	6.7×10^6	−10.00	−4.3	**1.8×10^{-2}**
Galβ4Glc (OS-3)	288	5.6×10^{10}	−14.25	−4.7	**3.3×10^{-2}**	7.1×10^7	−10.41	−17.9	-2.6×10^{-2}
	298	8.7×10^7	−10.74	−4.7	**2.0×10^{-2}**	1.5×10^7	−9.85	−17.9	-2.7×10^{-2}
	308	4.8×10^7	−10.90	−4.7	**2.0×10^{-2}**	1.7×10^7	−10.26	−17.9	-2.5×10^{-2}
	318	4.1×10^7	−11.15	−4.7	**2.0×10^{-2}**	2.6×10^6	−9.39	−17.9	-2.7×10^{-2}
Gal6Sβ4Glc (OS-4)	288	1.3×10^8	−10.77	−15	-1.5×10^{-2}	1.4×10^6	−8.16	−20	-4.1×10^{-2}
	298	8.0×10^6	−9.47	−15	-1.9×10^{-2}	0.22×10^6	−7.32	−20	-4.3×10^{-2}
	308	2.2×10^7	−10.41	−15	-1.5×10^{-2}	0.15×10^6	−7.34	−20	-4.1×10^{-2}
	318	1.2×10^7	−10.35	−15	-1.5×10^{-2}	6.9×10^6	−10.02	−20	-3.1×10^{-2}
Galβ4GlcNac (OS-5)	288					1.2×10^7	−9.37	−7.3	**5.5×10^{-3}**
	298	9.4×10^7	−10.94	−4.2	**2.3×10^{-2}**	3.0×10^6	−8.68	−7.3	**3.6×10^{-3}**
	308	7.2×10^7	−11.14	−4.2	**2.3×10^{-2}**	1.8×10^7	−10.28	−7.8	**8.0×10^{-3}**
	318	6.1×10^7	−11.40	−4.2	**2.3×10^{-2}**	2.8×10^6	−9.44	−7.3	**5.2×10^{-3}**
Galβ4GlcNAc6S (OS-6)	288					1.3×10^8	−10.74	−23.4	-4.4×10^{-2}
	298	2.8×10^7	−10.23	−5.6	**1.5×10^{-2}**				
	308	1.7×10^7	−10.26	−5.6	**1.5×10^{-2}**	4.9×10^6	−9.49	−23.4	-4.5×10^{-2}
	318	1.6×10^7	−10.54	−5.6	**1.5×10^{-2}**	3.3×10^6	−9.55	−23.4	-43×10^{-2}
Galβ3GlcNAc (OS-7)	288	7.7×10^8	−11.79	−20	-2.9×10^{-2}	1.5×10^5	−6.85	−7.2	-1.2×10^{-3}
	298	1.9×10^8	−11.36	−20	-2.9×10^{-2}	1.8×10^4	−5.3S	−7.2	-4.5×10^{-3}
	308	7.7×10^7	−11.19	−20	-2.9×10^{-2}	6.4×10^5	−6.62	−7.2	-1.3×10^{-3}
Galβ3GalNAc (OS-9)	288	2.4×10^{13}	−17.74	−72.3	−0.19	8.2×10^7	−10.5	−11.3	-2.8×10^{-3}
	298	1.1×10^{11}	−15.12	−72.3	−0.19				
	308	2.1×10^{10}	−14.63	−72.3	−0.19	1.4×10^8	−11.55	−11.3	0.78×10^{-3}
	318	7.8×10^7	−11.56	−72.3	−0.19	7.6×10^6	−10.08	−11.3	-3.9×10^{-3}
Neu5Acα6GalNAc (OS-18)	288	1.1×10^7	−9.33	**1.1**	**3.6×10^{-2}**	1.2×10^6	−8.05	−27.4	-6.7×10^{-4}
	298	2.3×10^8	−11.47	**1.1**	**4.2×10^{-2}**	1.3×10^5	−7.02	−27.4	-6.8×10^{-2}
	308	5.7×10^6	−9.58	**1.1**	**3.5×10^{-2}**	54×10^4	−6.71	−27.4	-6.7×10^{-2}
	318	4.4×10^7	−11.20	**1.1**	**3.9×10^{-2}**	7.5×10^6	−10.07	−27.4	-5.4×10^{-2}
Kdnα6Galβ4Glc (OS-19)	288	2.8×10^7	−9.87	−7.4	**0.86×10^{-2}**	5.0×10^6	−8.89	−12.9	-1.4×10^{-2}
	298	1.9×10^7	−9.97	−7.4	**0.86×10^{-2}**	7.4×10^6	−9.43	−12.9	-1.2×10^{-2}
	308	1.2×10^7	−10.04	−7.4	**0.86×10^{-2}**	1.62×10^6	−88.1	−12.9	-1.3×10^{-2}
	318	5.0×10^{11}	−17.13	−7.4	**3.1×10^{-2}**	0.77×10^6	−8.62	−12.9	-1.3×10^{-2}
Neu5Gcα6Galβ4Glc (OS-20)	288	1.0×10^8	−10.62	−13.1	-0.86×10^{-2}	3.2×10^6	−8.63	−12.7	-1.4×10^{-2}
	298	3.3×10^7	−10.32	−13.1	-0.93×10^{-2}	1.7×10^6	−8.56	−12.7	-1.4×10^{-2}
	308	7.2×10^6	−9.73	−13.1	-1.1×10^{-2}	1.2×10^6	−8.64	−12.7	-1.3×10^{-2}
Neu5Acα6Galβ4Glc (OS-21)	288	115×10^8	−10.69	−12.9	-7.7×10^{-3}	4.2×10^7	−10.11	−16	-2.0×10^{-2}
	298	3.6×10^7	−10.40	−12.9	-8.4×10^{-3}	2.9×10^6	−8.87	−16	-2.4×10^{-2}
	308	2.2×10^7	−10.42	−12.9	-8.1×10^{-3}	1.7×10^7	−10.25	−16	-1.9×10^{-2}
	318	1.34×10^7	−10.44	−12.9	-7.7×10^{-3}	1.26×10^6	−8.93	−16	-2.2×10^{-2}
Neu5Acα6Galβ4GlcNAc (OS-22)	288	3.8×10^7	−10.05	−10.4	-1.2×10^{-3}	6.8×10^6	−9.06	−14.6	-1.9×10^{-2}
	298	3.0×10^7	−10.25	−10.4	-0.49×10^{-3}	8.8×10^6	−9.53	−14.6	-1.7×10^{-2}
	308	1.17×10^7	−10.03	−10.4	-1.2×10^{-3}	3.1×10^6	−9.21	−14.6	-1.8×10^{-2}
	318	5.9×10^7	−11.38	−10.4	-3.1×10^{-3}	0.65×10^6	−8.51	−14.6	-1.9×10^{-2}
Neu5Acα6Galβ4GlcNAc6S (OS-23)	298	1.5×10^7	−9.84	−8.5	**4.5×10^{-3}**	1.9×10^6	−8.60	−12.6	-1.3×10^{-2}
	308	8.5×10^6	−9.83	−8.5	**4.3×10^{-3}**	1.1×10^6	−8.56	−12.6	-1.3×10^{-2}
	318	6.1×10^6	−9.94	−8.5	**4.5×10^{-3}**	0.49×10^6	−8.33	−12.6	-1.3×10^{-2}
Neu5Acα3Galβ3GlcNAc (OS-24)	288	1.35×10^8	−10.78	−10.8	-0.56×10^{-4}	0.46×10^5	−6.18	−16.5	-3.6×10^{-2}
	298	1.0×10^8	−10.98	−10.8	6.0×10^{-4}	0.21×10^5	−5.94	−16.5	-3.5×10^{-2}
	308	2.9×10^7	−10.58	−10.8	-7.1×10^{-4}	0.07×10^5	−5.46	−16.5	-3.6×10^{-2}
	318	2.9×10^7	−10.93	−10.8	4.0×10^{-4}	1.6×10^7	−10.57	−16.5	-1.9×10^{-2}

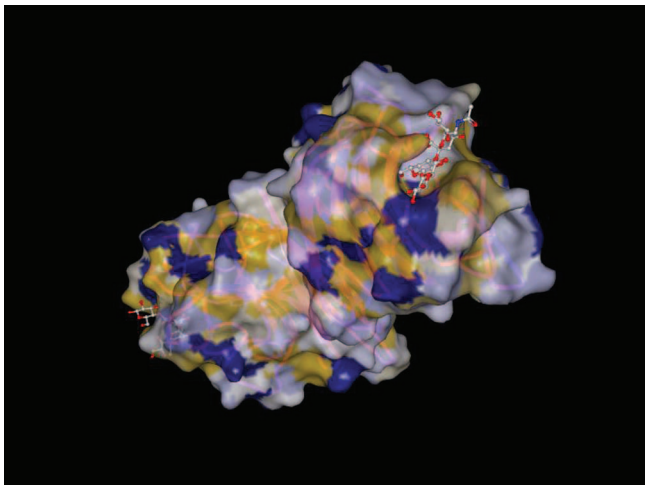

FIG. 6. Structure of MAA in complex with OS-11 (Neu5Acα2-3Galβ1-4Glc or α2-3-linked sialyllactose) determined from X-ray crystallography data.[27] The carbohydrate binding site consists of a deep cleft that accommodates the three monosaccharide residues of the sialyllactose. The central galactose sits in the primary binding site in an orientation that has not been observed previously in other legume lectins. The carboxyl group of sialic acid establishes a salt bridge with a lysine side chain. The glucose residue is very efficiently docked between two tyrosine aromatic rings. We suggest that the structured water layer over the hydrophobic portion of the pocket (yellow) is responsible for a large entropy gain in MAA-sialyllactosamine as well as MAA-sialyllactose complex formation as shown in Table II.

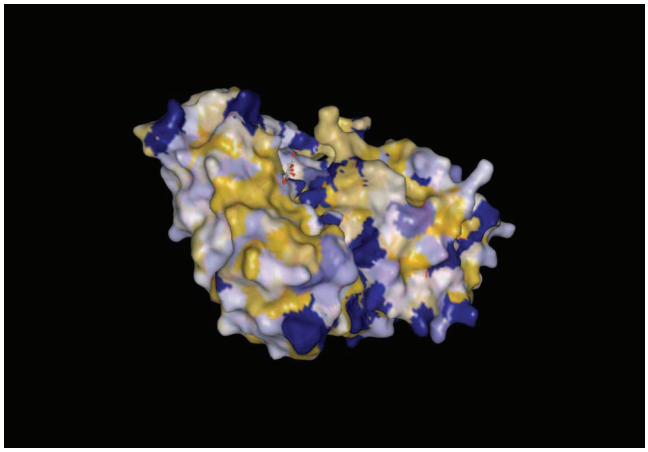

FIG. 7. Structure of RCA in complex with OS-1 (Galβ or β-galactose) determined from X-Ray crystallography data.[29] The carbohydrate binding site is near a deep cleft that can accommodate more than one monosaccharide residue.

ACKNOWLEDGMENTS

This work was supported by NIH Grant Nos. R01HG003827 (X.D.Z.), R01GM076360-04S1 and R01HD065122 (X.C.).

[1]G. A. Bezerra, E. Dobrovetsky, R. Viertlmayr, A. Dong, A. Binter, M. Abramic, P. Macheroux, S. Dhe-Paganon, and K. Gruber, Proc. Natl. Acad. Sci. U.S.A. **109**, 6525 (2012).
[2]A. L. Creagh, E. Ong, E. Jervis, D. G. Kilburn, and C. A. Haynes, Proc. Natl. Acad. Sci. U.S.A. **93**, 12229 (1996).
[3]K. Datta, A. J. Wowor, A. J. Richard, and V. J. LiCata, Biophys. J. **90**, 1739 (2006).
[4]N. Georgelis, N. H. Yennawar, and D. J. Cosgrove, Proc. Natl. Acad. Sci. U.S.A. **109**, 14830 (2012).
[5]R. R. Hantgan, D. S. Lyles, T. C. Mallett, M. Rocco, C. Nagaswami, and J. W. Weisel, J. Biol. Chem. **278**, 3417 (2003).
[6]J. Kang and J. Rebek, Nature (London) **382**, 239 (1996).
[7]O. Kartal, S. Mahlow, A. Skupin, and O. Ebenho, Mol. Syst. Biol. **7**, 542 (2011).
[8]F. Khan, S. M. Gaikwad, and M. I. Khan, Asian J. Biochem. **4**, 106 (2009).
[9]O. Indsgauld, E. P. Khare, M. Bach, and R. U. Lemieux, Can. J. Chem. **63**, 2653 (1985).
[10]H. Beierbeck, L. T. J. Delbaere, M. Vandonselaar, and R. U. Lemieux, Can. J. Chem. **72**, 463 (1994).
[11]R. U. Lemieux, Acc. Chem. Res. **29**, 373 (1996).
[12]R. P. Rand, N. L. Fuller, P. Butko, G. Francis, and P. Nicholls, Biochemistry **32**, 5925 (1993).
[13]H. J. Wittmann, R. Seifert, and A. Strasser, Mol. Pharmacol. **76**, 25 (2009).
[14]F. L. Yin, R. Cao, A. Goddard, Y. H. Zhang, and E. Oldfield, J. Am. Chem. Soc. **128**, 3524 (2006).
[15]M. A. Schwaller, G. Dodin, and J. Aubard, Biopolymers **31**, 519 (1991).
[16]M. W. Freyer and E. A. Lewis, Methods Cell Biol. **84**, 79 (2008).
[17]M. M. Pierce, C. S. Raman, and B. T. Nall, Methods **19**, 213 (1999).
[18]M. H. Chiu and E. J. Prenner, J. Pharm. Bioallied. Sci. **3**, 39 (2011).
[19]J. P. Landry, Y. Y. Fei, and X. D. Zhu, Assay Drug Dev. Technol. **10**, 250 (2012).
[20]Y. Y. Fei, A. Schmidt, G. Bylund, D. X. Johansson, S. Henriksson, C. Lebrilla, J. V. Solnick, T. Borén, and X. D. Zhu, Anal. Chem. **83**, 6336 (2011).
[21]Y. Y. Fei, J. P. Landry, Y. S. Sun, X. D. Zhu, X. B. Wang, J. T. Luo, C. Y. Wu, and K. S. Lam, J. Biomed. Opt. **15**, 016018 (2010).
[22]Y. Y. Fei, J. P. Landry, Y. S. Sun, X. D. Zhu, J. T. Luo, X. B. Wang, and K. S. Lam, Rev. Sci. Instrum. **79**, 013708 (2008).
[23]Y. Y. Fei, Y. S. Sun, Y. H. Li, K. Lau, H. Yu, H. A. Chokhawala, S. S. Huang, J. P. Landry, X. Chen, and X. D. Zhu, Mol. BioSys. **7**, 3343 (2011).
[24]J. P. Landry, Y. Y. Fei, and X. D. Zhu, Int. Drug Discov. **6**, 8 (2012).
[25]Y. S. Sun, J. P. Landry, Y. Y. Fei, X. D. Zhu, J. T. Luo, X. B. Wang, and K. S. Lam, Langmuir **24**, 13399 (2008).
[26]S. R. Haseley, P. Talaga, J. P. Kamerling, and J. F. G. Vliegenthart, Anal. Biochem. **274**, 203 (1999).
[27]A. Imberty, C. Gautier, J. Lescar, S. Pérez, L. Wyns, and R. Loris, J. Biol. Chem. **275**, 17541 (2000).
[28]L. Maveyraud, H. Niwa, V. Guillet, D. I. Svergun, P. V. Konarev, R. A. Palmer, W. J. Peumans, P. Rougé, E. J. M. Van Damme, C. D. Reynolds, L. Mourey, Proteins **75**, 89 (2009).
[29]A. G. Gabdoulkhakov, Y. Savochkina, N. Konareva, R. Krauspenhaar, S. Stoeva, S. V. Nikonov, W. Voelter, C. Betzel, A. M. Mikhailov, Protein Data Base ID: 1RZO, 2004.